Optics Letters

High-average-power single-longitudinal-mode pulse laser based on a pulse saturation seed-injection locking OPO

Jiliang Qin,[1,2] Jiaqi Song,[1] Xuechen Cao,[1] Donglin Cheng,[1] and Huadong Lu[1,2,*]

[1]State Key Laboratory of Quantum Optics and Quantum Optics Devices, Institute of Opto-Electronics, Shanxi University, Taiyuan 030006, China
[2]Collaborative Innovation Center of Extreme Optics, Shanxi University, Taiyuan 030006, China
*luhuadong@sxu.edu.cn

Received 16 August 2023; revised 3 September 2023; accepted 4 September 2023; posted 5 September 2023; published 18 September 2023

A high-average-power and narrow-linewidth nanosecond (ns) pulse 824 nm laser is a crucial source for the generation of deep-ultraviolet (DUV) 248 nm laser by means of the sum-frequency process with the 354.5 nm laser. To this purpose, in this Letter, we present a seed-injection-locked high-average-power ns pulse single-longitudinal-mode (SLM) 824 nm laser. By developing a novel, to the best of our knowledge, pulse-saturated seed-injection locking method, disturbance of the pulse laser on the locking of the injected seed laser is successfully eliminated. As a result, the output power of 824 nm laser is up to 21.2 W at the incident pump power of 48.1 W, and the pulse width is 15 ns. Especially, the signal-to-noise ratio of the detected modulated sideband signal exceeds 28 dB, which ensures that the achieved linewidth of the 824 nm laser is as narrow as 38.8 MHz. These results demonstrate the potential of the proposed pulse saturation seed-injection locking OPO cavity for high-power and narrow-linewidth laser applications. © 2023 Optica Publishing Group

https://doi.org/10.1364/OL.503195

Optical parametric oscillator (OPO) pumped by a pulsed solid-state laser has garnered significant interest due to its broad spectral ranges as well as high conversion efficiency and is applied in lots of fields including time-resolved characterization [1], high-resolution spectroscopy [2], nonlinear imaging of various species [3], and differential absorption lidar [4]. Especially, in order to obtain a stable near-infrared laser which is a crucial source for the generation of the deep-ultraviolet (DUV) 248 nm laser by means of the sum-frequency process with the 354.5 nm laser, a green-pumped OPO is the most attractive candidate, where the LiB_3O_5 (LBO), BBO, BIBO, and periodic poled crystals (PPLT, PPLN, and PPKTP) often act as the nonlinear media. However, the required minimum pulse peak power is relatively high for the BBO and BIBO crystals due to the employed critical phase-matching conditions, and the photo-refractive or photochromic damage of the most common periodically poled crystals is prone to restrict the average power of the obtained near-infrared laser. In Stark contrast, the LBO nonlinear crystal has proven exceptionally damage resistant and absorption free, thus is suitable for high-power OPO which are otherwise damage limited. In 2005, based on a single noncritical phase-matching LBO crystal, Li *et al.* reported an 18-W ns OPO around 860 nm and also found that the poor pump beam quality could not influence the output power and optical conversion of the achieved OPO [5], which supplies a good reference to design a stable high-power near-infrared OPO. Furthermore, to attain a single-longitudinal-mode (SLM) OPO, a volume Bragg grating or a mode-selector including birefringent filters and etalon are employed [6], but these components can introduce an insertion loss and further decrease the output power. Additionally, the damage threshold of the components can also restrict the output power. On the contrary, the seed-injection locking based on the Pound–Drever–Hall (PDH) is free of the loss, which pays the way for achieving a high-power OPO with narrow linewidth. However, when a continuous-wave (CW) single-frequency laser beam is injected as the seed light into the resonator of a pulsed OPO, high intensity of the achieved pulse laser can saturate the adopted detector and produce a large glitch in the error signal [7]. At the same time, a large peak power difference between the oscillating pulse laser in the OPO and the injected seed laser can result in the error signal to be drowned by the impulse noise, especially when the frequency of the higher harmonic of the pulse signal is close to the modulation frequency. In this case, direct detection becomes helpless because its significant noise leads to a low signal-to-noise ratio (SNR) of the error signal. To mitigate the influence of pulsed light on the error signal, Tomita *et al.* developed a detector based on a synchronous switch in 2008 [8,9]. Specifically, the detector is deactivated during the presence of the pulsed laser and activated when only a seed laser is present. At this time, although the SNR of the error signal is greatly improved because of the absence of the pulse laser, switch process can still introduce extra noise to the error signal, which leads to the developed detector not satisfying the requirement of the high-precision seed-injection locking of the OPO. Additionally, the switching system necessitates the addition of supplementary components and modules, which significantly amplifies the complexity of the locking system, particularly in the case of ns pulses with narrow pulse widths, which imposes stringent demands on the speed and noise of the switching system.

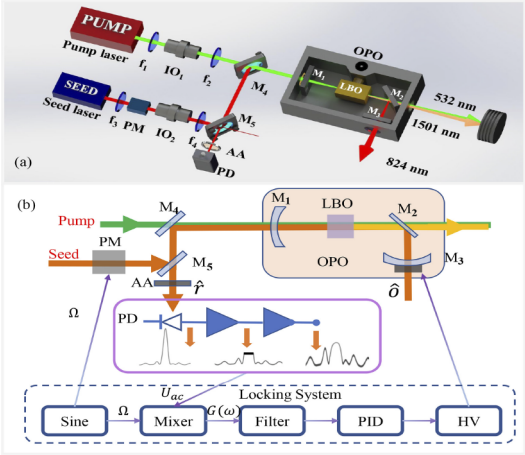


Fig. 1. (a) Schematic diagram of the designed injection-seed OPO setup and (b) Schematic diagram of the PSD locking program.

In this manuscript, we propose a novel pulse laser saturation seed-injection locking method for achieving a high-power pulse SLM OPO. Based on developing a photodetector for pulse laser saturation detection (PSD), a seed-injected SLM 824 nm OPO with the output average power of 21.2 W based on a noncritical phase-matching LBO crystal is realized. Especially, during the seed-injection locking process, the influence of pulse-laser intensity on the SNR of an error signal is eliminated. Consequently, the obtained error signal for OPO locking exhibits a high SNR of up to 28 dB, and the linewidth of the achieved OPO is as narrow as 38.8 MHz.

The experimental setup and the designed high-power SLM OPO are depicted in Fig. 1(a). In order to achieve a SLM 824 nm OPO, a homemade pulse 532 nm laser with a repetition frequency of 50 kHz and a pulse width of 15 ns was firstly employed to pump the designed OPO. The pump laser beam collimated by a lens f_1 with a focal length of 200 mm was focused to a spot with the radius of 67 um by the lens f_2 with the focal length of 150 mm and coupled into the resonator of the OPO. The resonator of the designed OPO was an L-shape folded standing-wave cavity consisting of two concave–convex mirrors (M_1 and M_3) and a plane mirror (M_2), which was beneficial to leak the residual pump laser and the generated idler laser from M_2. The length of the resonator was 206.3 mm. The curvature radius of convex and concave surfaces for both M_1 and M_3 were −100 mm and 100 mm, respectively. In order to increase the optical conversion efficiency, M_1 was coated with an HR film at 824 nm and an HT film at 532 nm, while M_2 was coated with an HR film at 824 nm and an HT film at 532 nm and 1501 nm. The output coupling mirror M_3 was coated with 20% transmission film for 824 nm light beam and glued to a piezoelectric transducer (PZT) for cavity-length scanning and locking. A noncritical phase matching LBO crystal coated with anti-reflection films at 532 nm and 824 nm was adopted in the experiment to generate signal and idler light beams. The cross section and length are 3 mm x 3 mm and 30 mm, respectively. It was placed at the beam waist between M_1 and M_3. After all elements were aligned, the output wavelength of the signal and idler light beams generated by the OPO can be changed by scanning the temperature of the LBO crystal. Especially, when the temperature of the LBO crystal was controlled to 126 °C, the center wavelength of signal light was 824 nm. In addition, a homemade single-frequency CW tunable Ti:sapphire (Ti:S) laser was employed to act as the seed laser to narrow the linewidth of the OPO. The seed laser was collimated and focused to a spot with the radius of 83.7 um by another two lens f_3 and f_4 with focal lengths of 200 mm and 120 mm, respectively. In order to eliminate the influence of the reflected laser on the pump and seed lasers, two isolators (IO_1 and IO_2) were used in the light path of pump and seed laser beams.

To achieve the stable seed-injection locking of the OPO, a phase modulator (PM) with the low residual amplitude modulation was inserted into the light path of the seed laser. In order to prevent the frequencies of the modulation signal and the high-order harmonic of the pulsed laser from coincident and further influence of the SNR of the sideband signal, a modulation signal with the frequency of 31.32 MHz was loaded onto PM to modulate phase of the seed laser. In order to extract error signal with high SNR, after the modulated seed laser was reflected and coupled into the resonator of the OPO by both M_5 coated with the 95% reflecting film for 824 nm and M_4 coated with HR film at 824 nm and HT film at 532 nm, the reflected seed laser from M_1 was used to extract the error signal, because the power of the pulsed laser output from M_3 was much greater than that leaked from M_1, while the sideband signal power of the reflected laser from OPO is equivalent to that of the transmitted. On this basis, a pulse saturation injection locking method was further developed, which was depicted in Fig. 1(b).

The optical field $\hat{r}$ injected into the PD can be expressed as

$$E_r(t) \approx \sqrt{r_{M_5}\eta}\{E_{in}[F(\omega)J_0(\beta)e^{i\omega t} + F(\omega+\Omega)J_1(\beta)e^{i(\omega+\Omega)t} - F(\omega-\Omega)J_1(\beta)e^{i(\omega-\Omega)t}] + \sqrt{T_1/T_3}E_n(t)e^{i\omega_n t}\}, \quad (1)$$

where r_{M_5} is the reflectivity of M_5, η is the transmittance of adjustable attenuator (AA), $E_{in}$is the amplitude of seed laser, $F(\omega)$ is the OPO reflection coefficient, an ω and ω_n are the frequencies of seed laser and generated pulsed laser, respectively. J_0, J_1 are the Bessel function, β is the modulation coefficient, ω is the modulation frequency, and $E_n(t)$ is the generated pulsed light. The power of optical field $\hat{r}$ can be expressed as

$$P_r(t) \approx P_0 + P_\Omega + P_n(\omega_n, t), \quad (2)$$

where

$$P_0 = P_c|F(\omega)|^2 + P_s\{|F(\omega+\Omega)|^2 + |F(\omega-\Omega)|^2\},$$
$$P_c = r_{M_5}\eta(E_{in}J_0(\beta))^2, P_s = r_{M_5}\eta(E_{in}J_1(\beta))^2,$$
$$P_\Omega = 2\sqrt{P_cP_s}\{\mathrm{Re}[G(\omega,\Omega)]\cos\Omega t + \mathrm{Im}[G(\omega,\Omega)]\sin\Omega t\},$$
$$G(\omega,\Omega) = F(\omega)F^*(\omega+\Omega) - F^*(\omega)F(\omega-\Omega),$$

P_0 is the DC term, P_Ω is the modulation signal, $P_n(\omega_n, t)$ is the pulse signal power, and $G(\omega,\Omega)$ is the error signal. When the resonant frequency of the OPO cavity is different from that of the seed laser, the pulse signal power can be expressed as

$$P_n(\omega_n, t) \approx \eta r_{M_5}|E_n(t)|^2 T_1/T_3, \quad (3)$$

where T_1 and T_3 are the transmittance of M_1 and M_3 at 824 nm, respectively. When the resonant frequency of the OPO is the same as that of the seed laser, the formula can be expressed as

$$P_n(\omega,t) \approx \eta r_{M_5}\{|E_n(t)|^2T_1/T_3 - |E_n(t)||E_{in}|F(\omega) J_0(\beta)\sqrt{T_1/T_3} - [\sqrt{T_1/T_3}E_n(t)F(\omega+\Omega)J_1(\beta) - \sqrt{T_1/T_3}E_n(t)F(\omega-\Omega)J_1(\beta)]2\cos\Omega t\}. \quad (4)$$

After the light field $\hat{r}$ is converted by the photodiode, the photocurrent is expressed as $I = RP_r(t)$, where R is photoelectric

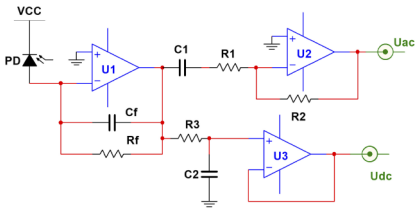


Fig. 2. The schematic diagram of the pulse saturation detector.

sensitivity. The DC term is $i_{DC} = RP_0$, and the modulation signal current is $i_\Omega = RP_\Omega$. The pulsed noise current is $i_n = RP_n(\omega_n, t)$.

From Eqs. (2) and (4), it is clear that the noise induced by the pulse laser $P_n(\omega_n, t)$ directly reduces the SNR of the error signal $G(\omega, \Omega)$, which can restrict the achievement of seed-injection locking. To address this issue, a photodetector for implementing the PSD is designed and illustrated in Fig. 2. Herein, the amplifiers U1 and U2 are OPA855, U3 is OP27, the trans-resistance Rf =5 kΩ, Cf = 0.5 pF, AC coupling capacitor C1 = 1 nF, R1 = 300 Ω, R2 = 5 kΩ, R3 = 10 kΩ, and C2 = 1 uF. The photodiode is s5973 (Hamamatsu). The bandwidth and the gain of the detector are 250 MHz and 83 kV/A, respectively. When a pulse laser and a seed laser simultaneously illuminate the photodiode, the sideband signal can obtain a remarkable transimpedance gain; meanwhile, the SNR is improved after the first stage of transimpedance amplification on the condition that the photocurrent signal of seed laser is unsaturated while that of the pulse laser saturates. By means of the second stage of AC amplification, the sideband signal is further amplified and the pulse signal is further saturated, which enables higher gain and SNR of the sideband signal. The U3 part is a follower, mainly used to monitor the DC signal which can show whether the seed laser is saturated or not.

Based on the developed PD, the output voltage signal U_{ac} can be expressed as

$$U_{out} = \begin{cases} -IZ_f, & I<I_{\max} \\ -U_{\max}, & I \geq I_{\max} \end{cases},$$
$$U_{ac} = \begin{cases} -U_{out}Z_2/Z_1, & |U_{out} + i_{DC}R_f|<U_{\max}Z_1/Z_2 \\ \pm U_{\max}, & |U_{out} + i_{DC}R_f| \geq U_{\max}Z_1/Z_2 \end{cases},$$

where $I_{\max}$ and U_{out} are input saturation current and output voltage of the amplifier U1, respectively, $U_{\max}$ is the saturation voltage of U1 and U2, Z_f is transimpedance, Z_1 is the impedance of R1 and C1, and Z_2 is the impedance of R2.

Before implementing the seed-injection locking, the light field $\hat{r}$ in both frequency and time domains was firstly measured by using the developed PD, and the measured results are depicted in Fig. 3. When the seed laser is far off-resonant with the resonator of the OPO, the time-domain saturation detection results shown by the curve i in Fig. 3(a) depict that the power of light field $\hat{r}$ is the sum of the seed and pulse laser beams. However, when the seed laser is resonant with the resonator of the OPO, interference occurs between the pulse and seed lasers. At this time, the power of the light field drops quickly to zero and then rapidly rises to the maximum at the rising edge of the pulse light, and the similar principle can also be observed at the falling edge, which is shown in the curve ii of Fig. 3(a), and the results shown in Fig. 3(a) are consistent with those of Eqs. (2)–(4). Figure 3(b) exhibits the measured frequency-domain signals of PSD for different injected optical powers of the PD, while the seed laser is resonant with the resonator of the OPO. In the experiment,

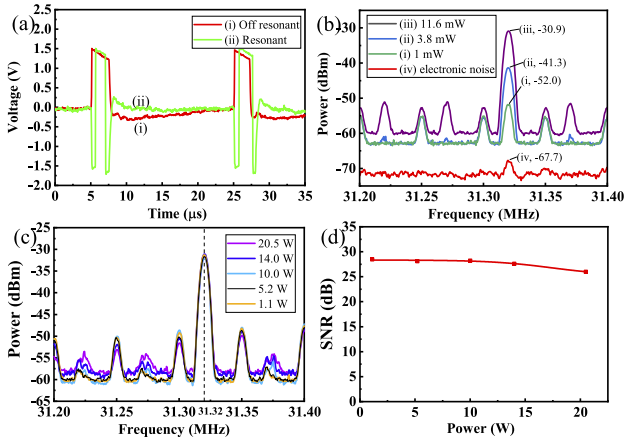


Fig. 3. The modulation signal and pulse signal in the time domain (a) and frequency domain (b). The results of the frequency-domain measurement (c) and SNRs (d) of sideband signals with different pulse optical power.

from the DC port of the PD, the measured CW laser saturation optical power of the light field $\hat{r}$ was 1.0 mW; meanwhile, the total power of $\hat{r}$ was 12.0 mW when the pump laser all injected. Then, by adjusting the AA to increase the power of $\hat{r}$ from 1 mW to 11.6 mW, the AC output of the PD U_{ac} was measured. The results depicted in Fig. 3(b) indicate that the amplitude of the modulation signal linearly increases with the injected optical power when the CW laser power is lower than the saturation optical power; meanwhile, the increase of the extra noise is basically negligible. Furthermore, to check the pulse-laser saturation characteristic of the developed PD, the power of the 824 nm pulse laser increased from 1.1 W to 20.5 W, while the power of the seed laser injected on PD is fixed to 1.0 mW. The measured results of the sideband signal are presented in Figs. 3(c) and 3(d). It can be found that the amplitude of the sideband signal and noise level basically do not change with the variation of the power of the pulse laser and the achieved SNR of sideband signal was always up to approximately 28 dB. The measured results depicted the good linearity and low noise characteristic of the PD for the PSD.

Next, depending on the developed PD, a high SNR error signal for seed laser injection locking was obtained after the detected signal U_{ac} mixed with a 31.32 MHz reference signal and subsequently performed 10 kHz low-pass filtering. When the PZT of OPO was driven by a triangular wave, the error signals were measured, and the results are represented in Fig. 4(a). It can be seen that even if the pulse light power is very high, the error signal of the PSD is basically the same as when only the seed light is present. For comparison, error signals without the PSD method were measured under the same measurement conditions, and the results are shown in Fig. 4(b). Curve iii is the error signal when there is only seed light, which is basically the same as the error signal adopting the PSD method. Curves i and ii are error signals when the output pulsed laser powers are 21.2 W and 5 W, respectively. It is obvious that the larger the pulse power, the worse the SNR of the error signal of the non-PSD.

Lastly, after the error signal was processed by a PID controller, a feedback signal was achieved. By loading this feedback signal on the PZT of the OPO resonator after a high-voltage amplifier, the resonator of OPO was successfully locked to the incident seed laser. Figure 5(a) illustrates the linewidth of the OPO before

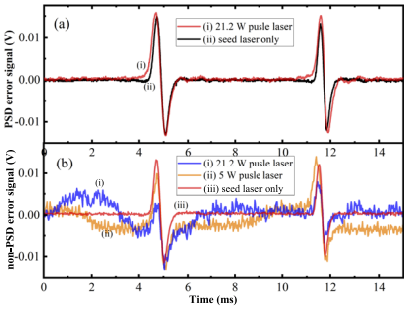


Fig. 4. (a) Error signal of the PSD. (b) Error signal of the non-PSD.

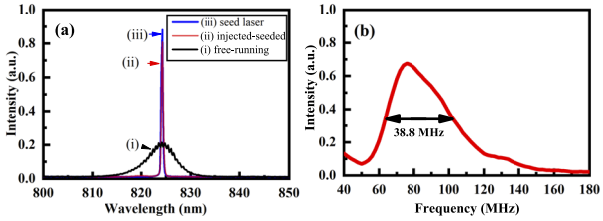


Fig. 5. Spectrum of the OPO output laser measured by the spectral analyzer (a) and by beating frequency with the seed laser (b).

and after the seed laser injection locking by using a spectrometer (AVANTES AvaSpec-ULS4096CL-EVO) with the precision of 0.5 nm. It is clear that the spectral width under free operation is as broad as 10 nm for the full width at half maximum (FWHM), which is successfully narrowed to lower than 0.5 nm (limited by the resolution of spectrometer) when the OPO is seed laser injection locked. In order to obtain the linewidth of the 824 nm pulse light more accurately, we beat the pulse laser with the seed laser after a 75 MHz frequency shift. Then the signal of beat frequency was measured, and after the Fourier analysis, the line width of FWHM was 38.8 MHz as shown in Fig. 5(b). On this basis, the output trend and stability of the achieved SLM OPO were also measured and recorded by a power meter as shown in Figs. 6(a) and 6(b). The measured threshold power of OPO was 7 W, and the maximum power of 21.2 W at an incident pump power of 48.1 W was achieved. According to Fig. 6(a), we believe that a higher output power can be expected if the higher incident pump power is established in the experiment. The slope efficiency was measured to be 54%, whereas the opto-optical conversion efficiency was determined to be 43.8%. The average power fluctuation of the output pulsed laser was ±0.62% within 2 h. At last, the pulse width and beam quality of the output pulsed laser were measured by a pulse detector and a beam quality analyzer, respectively, and the results are shown in Figs. 6(c) and 6(d), which indicate that the pulse width is 15 ns and the M^2 factors of the beam are calculated to be 1.21 and 1.29 in the x and y directions, respectively.

In this study, we propose a pulse-saturated seed-injection locking method and develop an OPO cavity based on LBO crystals to produce an 824 nm pulse laser with narrow linewidth and high power (21.2 W). In the experiment, we analyze the pulse saturation locking principle and design a photodetector to saturate the pulse noise and effectively capture the error signal for OPO

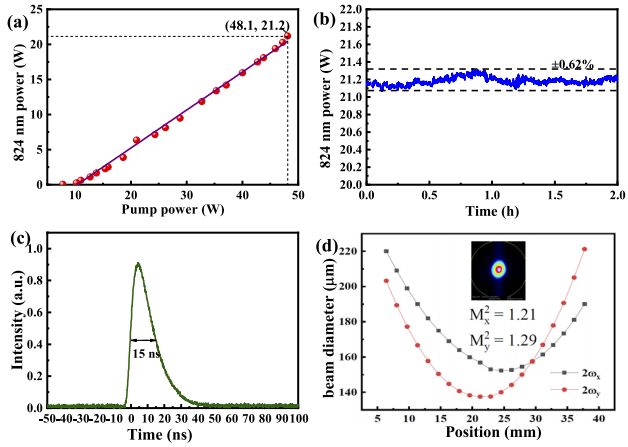


Fig. 6. (a) Output power of the 824 nm laser. (b) Power stability of the OPO output laser in 2 h. (c) The pulse width of the OPO laser. (d) The M^2 factors of the OPO output laser.

locking, which enabled us to achieve seed-injection locking and obtain the desired narrow-linewidth and high-power pulse laser. The proposed PSD technique has the characteristics of high SNR and basically ignoring pulsed laser, showing great potential in the generation of the pulsed laser with high power and narrow linewidth.

Funding. National Natural Science Foundation of China (61975100, 62027821, 62273361); National Key Research and Development Program of China (2022YFC2204003); Applied Basic Research Program of Shanxi Province (202103021221004, 202203021212481); Fund for Shanxi "1331 Project" Key Subjects Construction; Research Project Supported by Shanxi Scholarship Council of China (2022-015); Special fund for Science and Technology Innovation Teams of Shanxi Province (202204051002005); Shanxi Province Patent Conversion Project (202305007); The First Lab - National Innovation Center (Shanxi) Science and Technology Innovation Project.

Disclosures. The authors declare no conflicts of interest.

Data availability. Data underlying the results presented in this paper are not publicly available at this time but may be obtained from the authors upon reasonable request.

REFERENCES

1. J. Herz, V. Siffrin, A. E. Hauser, A. U. Brandt, T. Leuenberger, H. Radbruch, F. Zipp, and R. A. Niesner, Biophys. J. **98**, 715 (2010).
2. R. Klieber and D. Suter, Phys. Rev. B **73**, 094408 (2006).
3. H. Chen, H. Wang, M. N. Slipchenko, Y. Jung, Y. Shi, J. Zhu, K. K. Buhman, and J.-X. Cheng, Opt. Express **17**, 1282 (2009).
4. T. F. Refaat, S. Ismail, A. R. Nehrir, J. W. Hair, J. H. Crawford, I. Leifer, and T. Shuman, Opt. Express **21**, 30415 (2013).
5. H. Li, H. Zhang, Z. Bao, J. Zhang, Z. Sun, Y. Kong, Y. Bi, X. Lin, A. Yao, G. Wang, W. Hou, R. Li, D. Cui, and Z. Xu, Opt. Commun. **232**, 411 (2004).
6. S. G. Sabouri and A. Khorsandi, Opt. Quantum Electron. **49**, 358 (2017).
7. J. A. J. Fitzpatrick, O. V. Chekhlov, J. M. F. Elks, C. M. Western, and S. H. Ashworth, J. Chem. Phys. **115**, 6920 (2001).
8. H. Tomita, C. Mattolat, T. Kessler, S. Raeder, F. Schwellnus, K. D. A. Wendt, K. Watanabe, and T. Iguichi, J. Nucl. Sci. Technol. **45**, 37 (2008).
9. V. Sonnenschein, I. D. Moore, S. Raeder, M. Reponen, H. Tomita, and K. Wendt, Laser Phys. **27**, 085701 (2017).